

CONSTRAINTS ON PARAMETERS OF RADIATIVELY DECAYING DARK MATTER FROM THE GALAXY CLUSTER 1E 0657–56

A. BOYARSKY^{1,2,3}, O. RUCHAYSKIY⁴, AND M. MARKEVITCH^{5,6}

Draft version February 3, 2018

ABSTRACT

We derived constraints on parameters of a radiatively decaying warm dark matter particle, e.g., the mass and mixing angle for a sterile neutrino, using *Chandra* X-ray spectra of a galaxy cluster 1E 0657–56 (the “bullet” cluster). The constraints are based on nondetection of the sterile neutrino decay emission line. This cluster exhibits spatial separation between the hot intergalactic gas and the dark matter, helping to disentangle their X-ray signals. It also has a very long X-ray observation and a total mass measured via gravitational lensing. This makes the resulting constraints on sterile neutrino complementary to earlier results that used different cluster mass estimates. Our limits are comparable to the best existing constraints.

Subject headings: Dark matter — elementary particles — galaxies: clusters: individual (1E 0657–56) — line: formation — neutrinos — X-rays: galaxies: clusters — X-rays: individual (1E 0657–56)

1. STERILE NEUTRINO AS WARM DM CANDIDATES

A number of works appeared recently on the subject of a sterile (or *right-handed*) neutrino as a possible dark matter (DM) candidate (e.g., Asaka et al. 2005; Asaka & Shaposhnikov 2005; Abazajian 2006b,a; Boyarsky et al. 2006a,b,c,d,e; Asaka et al. 2006a; Shaposhnikov & Tkachev 2006; Riemer-Sørensen et al. 2006; Watson et al. 2006). The discovery of neutrino oscillations (see, e.g., Strumia & Vissani 2006 for a review) made the existence of a sterile neutrino quite plausible and spurred the interest in this candidate. Several factors make dark matter made of sterile neutrinos with a mass in the keV range particularly interesting:

(i) It is the lowest possible range of masses for fermionic DM. The Pauli exclusion principle applied to the DM particles in the halos of dwarf spheroidal galaxies (such as Draco or Ursa Minor) implies a lower bound on the particle mass $M_{\text{DM}} \gtrsim 350 \text{ eV}$ (Tremaine & Gunn 1979). Thus the sterile neutrino can be light enough to be a *warm* DM candidate (see below).

(ii) Warm DM with a keV mass can alleviate the problem of too many small subhalos inside the bigger dark matter halos, and too sharp central density peaks in the galaxy-sized DM halos predicted in the Cold Dark Matter scenario (Bode et al. 2001; Goerdt et al. 2006). For example, the flat central radial mass profile of the Fornax dwarf spheroidal galaxy (Goerdt et al. 2006; Strigari et al. 2006) can be explained if dark matter is warm with $M_{\text{DM}} \sim 2 \text{ keV}$.

(iii) Asaka et al. (2005) and Asaka & Shaposhnikov (2005) recently demonstrated that a simple extension of the Standard Model by three singlet fermions with masses smaller

than the electroweak scale can accommodate the data on neutrino masses and mixings, provides a candidate dark matter particle (in the form of the lightest sterile neutrino), and can explain the baryon asymmetry of the Universe. Such an extension (dubbed νMSM) can quantitatively explain these “beyond the Standard Model” phenomena within a single consistent framework. It should be tested observationally, and one such test is the search for the sterile neutrino DM.

(iv) For a DM particle with the mass in the keV range, one can obtain lower bounds on its mass by modeling the large scale structure formation. The power spectrum of the matter density fluctuations derived from the Lyman- α forest data in the SDSS, spanning redshifts $2.2 < z < 4.2$ (Seljak et al. 2006; Viel et al. 2006) constrains the mass of a warm DM particle to the range $\gtrsim 10 \text{ keV}$ ($\gtrsim 14 \text{ keV}$ in Seljak et al. (2006)). However, a more conservative analysis using only the higher spectral resolution Lyman- α data and lower redshifts gives $M_{\text{DM}} \gtrsim X \text{ keV}$ (Hansen et al. 2002; Viel et al. 2005).

(v) Sterile neutrinos with a keV mass would have other interesting astrophysical applications (e.g., Kusenko 2006b,a; Biermann & Kusenko 2006; Stasielak et al. 2006).

The sterile neutrino should possess a radiative decay channel (Pal & Wolfenstein 1982; Barger et al. 1995) (see §1.1 below). An emission line from neutrino decay has been searched for — so far unsuccessfully — in the X-ray spectra of various types of astrophysical objects, including clusters of galaxies (Abazajian et al. 2001b; Boyarsky et al. 2006c), the diffuse X-ray background (Dolgov & Hansen 2002; Boyarsky et al. 2006a), the DM halo of the Milky Way (Boyarsky et al. 2006d,e; Riemer-Sørensen et al. 2006), dwarf galaxies (Boyarsky et al. 2006d,e), and the M31 galaxy (Watson et al. 2006). Assuming that all of the dark matter is in the form of sterile neutrinos, nondetection of such a line places constraints on the mixing angle of the sterile neutrino as a function of mass in the range $1 \text{ keV} \lesssim M_s \lesssim 100 \text{ keV}$. To derive such constraints, one needs to know the mass of the DM in the field of view of the X-ray spectrometer, $M_{\text{DM}}^{\text{fov}}$ (eq. 2 below). There are several ways of deriving these masses:

¹ CERN, PH-TH, CH-1211 Geneva 23, Switzerland

² École Polytechnique Fédérale de Lausanne, Institute of Theoretical Physics, FSB/ITP/LPPC, BSP 720, CH-1015, Lausanne, Switzerland

³ On leave from Bogolyubov Institute of Theoretical Physics, Kyiv, Ukraine

⁴ Institut des Hautes Études Scientifiques, Bures-sur-Yvette, F-91440, France

⁵ Harvard-Smithsonian Center for Astrophysics, Cambridge, MA 02138, USA

⁶ Space Research Institute, Moscow, Russia

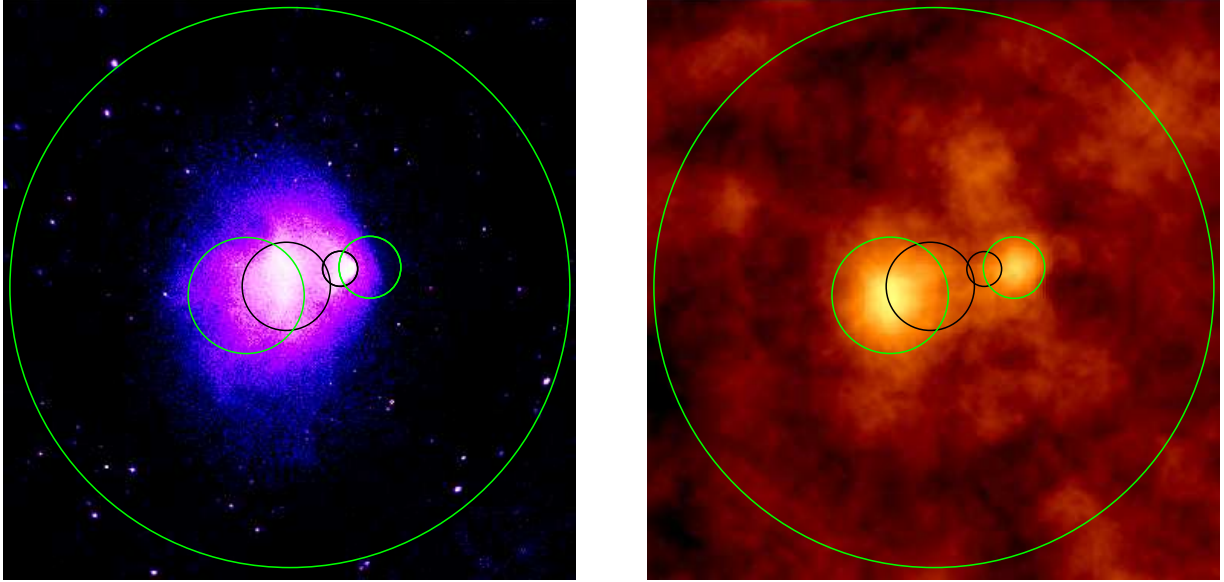


FIG. 1.— Regions used for extracting the X-ray spectra overlaid on a *Chandra* X-ray 0.8–4 keV image of 1E0657–56 (*left panel*) and its weak lensing mass map (Clowe et al. 2006) (*right panel*). The panel size is $12' \times 12'$. All point sources seen in the X-ray image are spatially excluded from the spectral analysis. The region that we refer to as SUB is the green circle centered on the western subcluster’s mass peak, excluding the smaller black circle encompassing most of the X-ray gas bullet. The region PEAKS is a combination of SUB and the green circle centered on the eastern mass peak, again excluding the corresponding X-ray peak (the bigger black circle). The region WHOLE is the big ($r = 6'$) green circle, excluding only the gas bullet (the smaller black circle).

(a) Modeling rotational curves of stars in galaxies or the velocity dispersion of galaxies in dynamically relaxed galaxy clusters;

(b) reconstructing the density and temperature profiles of the hot intergalactic gas in relaxed galaxy clusters using X-ray data and determining the total mass from the assumption of hydrostatic equilibrium (e.g., Cavaliere & Fusco-Femiano 1976; Bahcall & Sarazin 1977; Vikhlinin et al. 2006);

(c) For sufficiently distant ($z > 0.1$) clusters, gravitational lensing can be used (Bartelmann & Schneider 2001), which does not require a cluster to be relaxed.

All previous observational constraints were derived for nearby objects ($z \lesssim 0.01$), for which a combination of methods (a) and (b) provided the DM density distribution and $M_{\text{DM}}^{\text{fov}}$. It is important to cross-check these results using objects with masses determined by all methods, to minimize the systematic uncertainties inherent in each method.

In the present work, we use a distant object ($z = 0.296$, corresponding to the luminosity distance $D_L = 1.530$ Gpc for our adopted cosmology with $h = 0.7$, $\Omega_m = 0.3$ and $\Omega_\Lambda = 0.7$), whose mass is determined via weak and strong gravitational lensing (Clowe et al. 2006; Bradac et al. 2006). This method gives the total projected mass within a given region in the sky, eliminating a number of uncertainties of other methods. It is the only mass measurement method applicable to this cluster, which undergoes a violent merger. The merger has also resulted in a unique separation between the dark and visible matter (Clowe et al. 2006), which we will utilize below.

1.1. Radiative decay of sterile neutrinos

A dark matter composed of sterile neutrinos should not be completely “dark” (Dolgov & Hansen 2002; Abazajian et al. 2001b). The sterile neutrino possesses a radiative decay channel, decaying at a rate Γ into an active neutrino and a photon with energy $E = M_s/2$ (where M_s is the sterile neutrino mass). It is convenient to parameterize the interaction with the active neutrino in terms of the mixing angle $\sin^2(2\theta)$. The decay

rate Γ is then given by (Pal & Wolfenstein 1982; Barger et al. 1995):

$$\begin{aligned} \Gamma &= \frac{9 \alpha G_F^2}{1024 \pi^4} \sin^2(2\theta) M_s^5 \\ &= 1.38 \times 10^{-22} \sin^2(2\theta) \left[\frac{M_s}{1 \text{ keV}} \right]^5 \text{ s}^{-1}. \end{aligned} \quad (1)$$

For distant objects, the decay flux into a solid angle Ω_{fov} (the spectrometer’s field of view, FoV) is given by

$$F_{\text{DM}} = \frac{M_{\text{DM}}^{\text{fov}} \Gamma}{4\pi D_L^2} \frac{E}{M_s} \quad (2)$$

where $M_{\text{DM}}^{\text{fov}}$ is the total mass of DM within this solid angle. If the object is at a redshift z ,

$$\begin{aligned} F_{\text{DM}} &= 6.4 \left(\frac{M_{\text{DM}}^{\text{fov}}}{10^{14} M_\odot} \right) \left(\frac{100 \text{ Mpc}}{D_L} \right)^2 \\ &\times \sin^2(2\theta) \left[\frac{M_s}{1 \text{ keV}} \right]^5 \text{ keV cm}^{-2} \text{ s}^{-1}. \end{aligned} \quad (3)$$

Nondetection of any X-ray emission lines in the spectrum of a massive object that are not expected from its baryonic constituents (the hot intergalactic gas in the case of a galaxy cluster) can be used to place an upper limit on the flux from sterile neutrino decay. Eq. (3) can then be used to constrain the parameters M_s and θ .

2. THE 1E0657–56 CLUSTER

1E0657–56 is an interesting object for constraining the brightness of the neutrino line, for several reasons. Its total mass is directly measured from gravitational lensing (Clowe et al. 2006; Bradac et al. 2006). It also has a very long (450 ks) *Chandra* observation (Markevitch 2005), which provides a high-statistic X-ray spectrum. While formal constraints on the neutrino model that we will obtain below (§4)

TABLE 1
MASSES WITHIN SPECTRAL EXTRACTION REGIONS

Region	Total Mass, ^a $10^{15}M_{\odot}$	Gas mass, $10^{15}M_{\odot}$	DM mass, $10^{15}M_{\odot}$	area, ^b 10^{-7} sr
SUB	0.058	0.007	0.05	1.00
PEAKS	0.198	0.034	0.16	3.55
WHOLE	1.46	0.297	1.16	95.3

^a Masses from weak lensing

^b The solid angle of the region

are not significantly better than those previously derived from the nearby X-ray clusters Coma and Virgo (Boyarisky et al. 2006c), 1E 0657–56 provides a significant improvement in reliability, because of its directly measured total mass (whereas Coma and Virgo are both nearby unrelaxed systems, so their dark matter masses, and how much of it falls inside the instrument FoV, is uncertain).

A unique feature of 1E 0657–56 is a spatial separation between the peaks of gas and dark matter density belonging to the two subclusters (Clowe et al. 2006), caused by their merger in the plane of the sky (Fig. 1). This enables us to try to exclude the spatial regions with the highest thermal X-ray contamination (and thus minimize the uncertainty of modeling this component, see §3.1 below), while at the same time retaining the densest dark matter regions. Thus, we will use two regions in our X-ray analysis below, shown in Fig. 1. The region PEAKS takes advantage of the separation between the DM and gas and combines two circles centered on the mass peaks, excluding the two X-ray brightness peaks. We will also use a subregion of PEAKS that includes only the bullet subcluster mass peak, SUB, to illustrate the effects of uncertainties. The region WHOLE includes most of the cluster mass within $r = b' = 1.6$ Mpc (a still bigger region will increase uncertainties of the mass and the detector background), excluding only a small region at the X-ray brightness peak.

To calculate the dark matter mass within the spectral extraction regions, we integrated the weak lensing map of the projected total mass (Clowe et al. 2006) and subtracted a relatively small contribution from the intracluster gas. We note that the mass near the cluster center derived from weak lensing is lower by a factor of about 2 compared to that derived by Bradač et al., who combined weak and strong lensing data (but whose fit is in fact dominated by the strong lensing data). Some of this discrepancy is expected, because the weak lensing approximation breaks down near the peaks of massive clusters that produce strong gravitational arcs (such as both subclusters of 1E 0657–56); indeed, the peak densities in Clowe et al. (2006) are insufficient to produce arcs. Weak lensing is also insensitive to adding a constant mass sheet (Bartelmann & Schneider 2001). Strong lensing analysis may suffer from other types of uncertainties. The higher-mass Bradac et al. (2006) map is limited to the central $r = 1.5' - 2'$ region, insufficient for our purposes, so we chose to use the Clowe et al. (2006) mass map. This will result in conservative underestimates of the expected neutrino signal by a factor of up to 2. We will illustrate this uncertainty in the final results.

The gas mass within our spectral regions is estimated from a three-dimensional model fit to the *Chandra* X-ray brightness and temperature maps. The X-ray emissivity of a hot gas ($T \sim 8 - 20$ keV) in the *Chandra* energy band is determined mostly by the gas density, and depends weakly on temperature. Clusters are optically thin for X-rays, so in general, their gas density can be reconstructed very reliably for symmetric clusters.

The apparent axial symmetry of 1E 0657–56 allowed us to derive a gas model with a 10% accuracy Markevitch & et al. (2006). The gas contribution to the total mass in our spectral regions is about 25% (for the total mass from weak lensing), which we subtracted to obtain the dark matter masses given in Table 1. Given the small contribution of gas to the total mass, its uncertainty will be neglected.

3. DATA ANALYSIS

We use the deep *Chandra* (Weisskopf et al. 2002) ACIS-I observation of 1E 0657–56 described in Markevitch (2005); Markevitch & et al. (2006). The ACIS non-grating energy resolution is between 12%–4% (half-power line width $\Delta E/E$) in the $E = 1 - 8$ keV range. The X-ray spectra, the blank-sky background spectra, and ACIS responses (that include all instrument effects such as mirror effective area, detector efficiency and energy resolution, to be applied to a model spectrum in order to compare it to the data) were derived as described in Markevitch & et al. (2006) and Vikhlinin et al. (2006). Spectral fitting was performed using the XSPEC package (Arnaud 1996). The spectra for our three regions, SUB, PEAKS, and WHOLE, were well-fit (with reduced $\chi^2 \approx 1$ in all cases) with models consisting of one or several thermal plasma components (APEC, Smith et al. 2001) representing the multitemperature intracluster gas. A useful property of thermal spectra is that a continuous range of gas temperatures produces a spectrum that can be adequately fit with a sum of just several discrete temperatures. Models for all regions were modified at low energies by the Galactic absorption with $N_H = 4.6 \times 10^{20} \text{ cm}^{-2}$. An example of the fit for the region SUB is shown in Fig. 2; this fit has a reduced $\chi^2 = 0.98$ for 152 d.o.f.

None of the regions exhibits any emission lines other than those expected from hot gas (mostly the $E \simeq 6.7$ keV Fe line, redshifted to 5.2 keV). We use this fact to place constraints on the neutrino decay flux following the procedure previously used in this context by, e.g., Boyarisky et al. (2006a,c,d,e). In particular, for each energy bin in the 0.8–9 keV range, we added a narrow emission line (a Gaussian line much narrower than the detector spectral resolution) to the thermal model, re-fit the spectra, and calculated a statistical upper limit on the line flux by increasing the line normalization until χ^2 of the fit worsens by 9 (3σ or 99.7% confidence level). To obtain con-

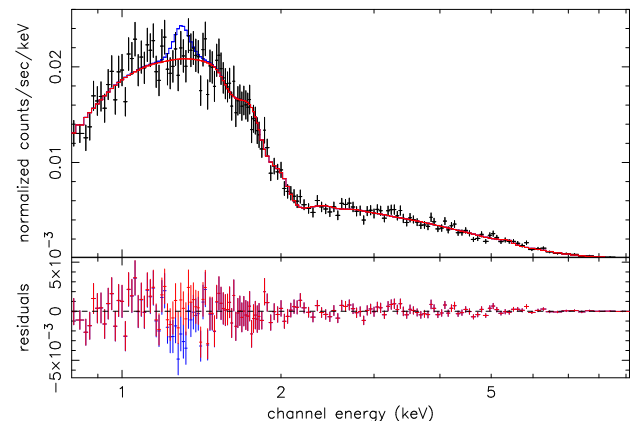


FIG. 2.— Spectrum for the SUB region with the best-fit APEC model shown in red. For illustration, we show an additional narrow line at $E = 1.3$ keV (blue model line and residuals), which worsens the fit at a 3σ level.

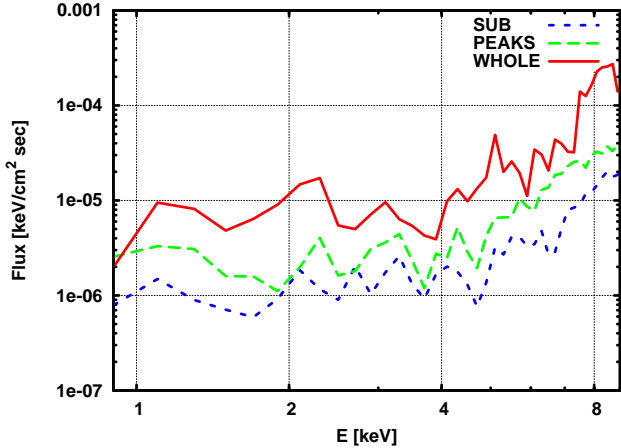


FIG. 3.— Statistical upper limits (3σ) for the flux in a nonthermal, narrow emission line as a function of line energy, for our fitting regions.

servative upper limits, we allowed as much freedom for the parameters of thermal model as possible, including allowing the heavy element abundances (that produce the thermal emission lines) to vary, thus letting the neutrino line mimic some of the thermal line flux at the respective energies. We note that the full number of counts in each bin (including the instrumental background) is sufficiently high to ensure the Gaussian statistics, and is much higher than the resulting limits on the line flux, so the use of $\Delta\chi^2$ is appropriate (cf. Protassov et al. 2002). An example of an emission line that would correspond to a 3σ upper limit is shown in Fig. 2, and the resulting statistical limits, in Fig. 3.

3.1. Systematic uncertainties

In addition to the statistical upper limits on the line flux, there are systematic uncertainties that has to be taken into account. First, the way how we normalize the ACIS background using the high-energy band Markevitch et al. (2003); Hickox & Markevitch (2006) results in a 3% uncertainty of the normalization at the useful energies. Because the ACIS detector background has several prominent emission lines, such incorrect normalization may, for example, hide an emission line coming from the sky, or create a spurious line. To take this into account, we varied the background normalization by 3% and repeated the fitting procedure. As expected, this leads to a noticeable increase of the allowed line flux only at rather high energies $E \gtrsim 6$ keV, where the background intensity increases steeply. For the region WHOLE, limits with nominal background normalization and those of for normalization changed by $\pm 3\%$ are shown in Fig. 4. These differences were added in quadrature to the statistical limits at each energy.

There is a more insidious uncertainty arising from the inaccuracies of calibration of the detector response and gain (the energy to spectral channel conversion). To assess this uncertainty, we have extracted a spectrum from the 880 ks ACIS observation of the very bright Perseus cluster, and fit it using the same calibration products (current as of summer 2006) and a model consisting of several thermal models as we use in this work, with all element abundances allowed to vary. The fit is shown in Fig. 5. Statistical errors in this dataset are mostly negligible. The fit shows systematic residuals at a 2–3% level of the model flux, some edge-like or even line-like, obviously caused by calibration inaccuracies (e.g., the

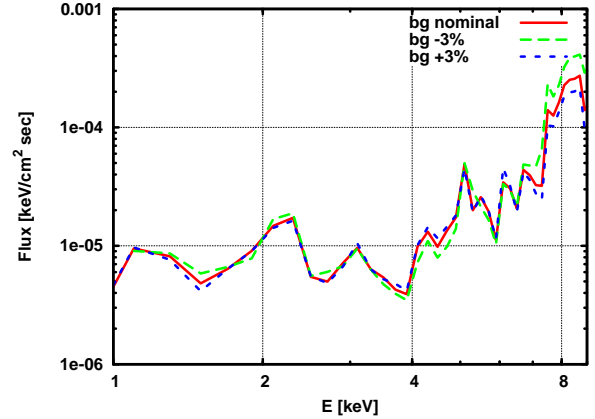


FIG. 4.— The effect of a $\pm 3\%$ systematic uncertainty in the ACIS background normalization for the region WHOLE on our line limits. It is significant for large regions and at high energies; for smaller regions such as SUB and PEAKS, it is negligible (not shown).

feature around $E = 2$ keV is obviously due to a gain error). To take this uncertainty into account, we added 3% of the thermal model flux contained within the width of a Gaussian line, in quadrature to the statistical limits on the line flux. The result of adding these uncertainties for regions WHOLE and SUB is shown in Fig. 6. As expected, this uncertainty contributes mostly at lower energies, where thermal emission is bright (at high energies, the increasing statistical uncertainty starts to dominate). This is the uncertainty that can be minimized by observing “dark” matter clumps, such as our gas-stripped subcluster.

Finally, the biggest uncertainty, unrelated to the X-ray data, comes from the factor of 2 difference between the cluster masses determined from the weak and strong gravitational lensing analyses Clowe et al. (2006); Bradac et al. (2006). We will include it in the plot with results below (Fig. 7b).

4. RESULTS

Using eq. (3) and masses from Table 1 (and, of course, the assumption that sterile neutrinos account for all of the dark matter), we convert upper limits on the neutrino line flux for our two regions into restrictions on sterile neutrino in the

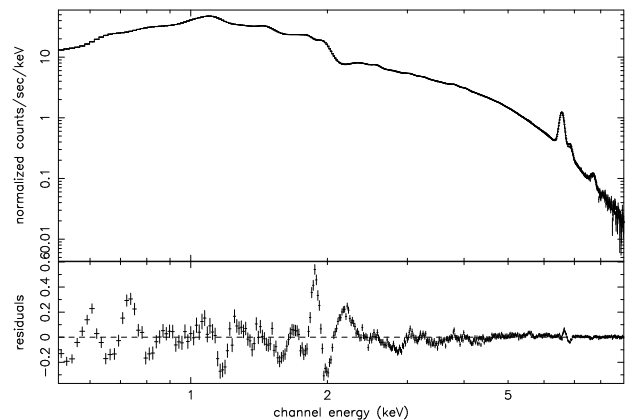


FIG. 5.— *Chandra* ACIS spectrum of the Perseus cluster from a 880 ks exposure, extracted from the $8' \times 8'$ central region, excluding the very center ($r < 1'$) with complex gas structure. The fit residuals illustrate the current calibration uncertainties. The residuals around 2–4 keV are 2–3%.

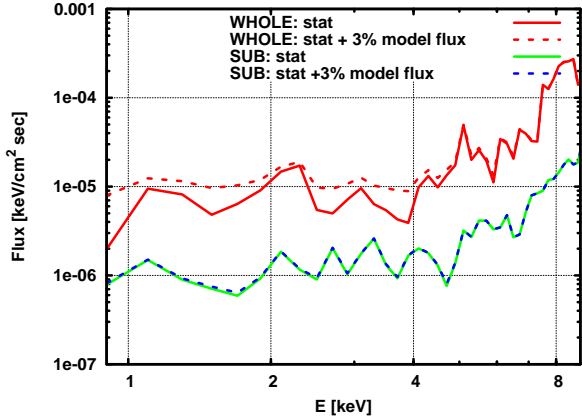


FIG. 6.— The effect of a 3% calibration uncertainty in the model flux (that can take the shape of spurious lines, see Fig. 5). It is significant for the line limits derived in regions with bright underlying X-ray emission (WHOLE), and negligible for regions avoiding the X-ray brightness peaks, such as (SUB).

$M_s - \sin^2(2\theta)$ plane. They are shown in Fig. 7. The strongest constraint comes from the region WHOLE — the bigger mass of DM within the field of view turns out to offer a greater advantage than the reduced thermal contamination at the gas-stripped DM peaks. For the SUB and PEAKS regions, we plot constraints for the conservative (perhaps excessively so) DM mass estimate from weak gravitational lensing (Fig. 7a) along with a stronger estimate for the higher strong lensing mass (Fig. 7b).

Although on average these results are about an order of magnitude weaker (in terms of $\sin^2[2\theta]$) than other recent limits (e.g., Boyarsky et al. 2006d; Watson et al. 2006)⁷ or more recent results (Boyarsky et al. 2006e), they serve as an important cross-check. First, they are obtained from an object with $z \sim 0.3$, while previous results (Boyarsky et al. 2006a,c,d; Riemer-Sørensen et al. 2006; Watson et al. 2006) were obtained for objects with $z \lesssim 0.01$ ⁸. Furthermore, the DM mass was determined via gravitational lensing, a method not applicable for nearby objects. This is important, as different mass measurement methods are subject to different uncertainties, and using an object such as 1E 0657–56 makes the constraints more robust.

4.1. Dodelson-Wilson scenario

Assuming that sterile neutrinos constitute all the DM and that they are produced in the early Universe via mixing with active neutrinos only, one should expect a relation between the mass of sterile neutrino and its mixing

⁷ We note that the M31 constraints presented in Watson et al. (2006) (as a straight line in the $M_s - \sin^2(2\theta)$ plane) should be very qualitative at $M_s \gtrsim 10 - 12$ keV. They must worsen as our limits do, since the XMM effective area rapidly declines at the corresponding energies, similarly to *Chandra*'s.

⁸ When this work was in final preparation, a

angle (Dodelson & Widrow 1994; Dolgov & Hansen 2002; Abazajian et al. 2001a; Abazajian 2006b). Combined with observational restrictions on the DM decay emission, this provides an upper bound on the sterile neutrino mass.

However, as sterile neutrinos do not thermalize in the early Universe, any such model relies on a number of assumptions (including initial conditions at temperatures $\gtrsim 1$ GeV and the absence of entropy dilution) (Boyarsky et al. 2006d; Asaka et al. 2006a). To define the boundary conditions, the knowledge of some “beyond the ν MSM” physics is needed. For example, it was shown in Shaposhnikov & Tkachev (2006) that all of the DM sterile neutrinos could have been produced by interaction with inflation. In such a scenario, the mixing angle can be arbitrarily small, even zero. This means that the sterile neutrino mass and mixing angle are not necessarily related, contrary to the assumption used in recent literature (e.g., Abazajian 2006b; Watson et al. 2006). Upper limits on the neutrino mass placed in those works, based on the upper limits on the decay line flux, are not only model-dependent, but depend strongly on the initial conditions. Moreover, even assuming ad hoc initial conditions implying that there was no DM at the temperatures $\gtrsim 1$ GeV (which is hardly physically justified), the correct calculation of the production rate requires calculation of the non-perturbative QCD contributions, which is still a subject of discussion in the literature (Asaka et al. 2006a,b).

Nevertheless, for the sake of comparison with other works, the intersection of our constraints in Fig. 7a with the $M_s - \sin^2(2\theta)$ relation obtained in Abazajian (2006b) for the simplest DW model (with one sterile neutrino, assuming zero initial conditions and a particular form of QCD contribution) corresponds to an upper limit $M_s < 6.3$ keV.

We would like to thank A.Neronov, M.Shaposhnikov and I.Tkachev for useful discussions. OR was supported in part by the European Research Training Network contract 005104 “ForcesUniverse” and by a *Marie Curie International Fellowship* within the 6th European Community Framework Programme. MM acknowledges support from NASA contract NAS8-39073 and *Chandra* grant GO4-5152X.

preprint Riemer-Sorensen et al. (2006) appeared, in which a *Chandra* grating spectrum of the cluster A1835 ($z \simeq 0.25$) is analyzed. That analysis strongly underestimated the effect of the cluster angular extent on energy resolution of the grating spectrum, so we do not consider it here.

REFERENCES

- Abazajian, K. 2006a, Phys. Rev., D73, 063513, astro-ph/0512631
 —. 2006b, Phys. Rev., D73, 063506, astro-ph/0511630
 Abazajian, K., Fuller, G. M., & Patel, M. 2001a, Phys. Rev., D64, 023501, astro-ph/0101524
 Abazajian, K., Fuller, G. M., & Tucker, W. H. 2001b, Astrophys. J., 562, 593, astro-ph/0106002
 Arnaud, K. A. 1996, in A.S.P. Conference Serie, Vol. 101, Astronomical Data Analysis Software and Systems V, ed. G. H. Jacoby & J. Barnes (San Francisco, ASP), 17
 Asaka, T., Blanchet, S., & Shaposhnikov, M. 2005, Phys. Lett., B631, 151, hep-ph/0503065
 Asaka, T., Kusenko, A., & Shaposhnikov, M. 2006a, Phys. Lett., B638, 401, hep-ph/0602150
 Asaka, T., Laine, M., & Shaposhnikov, M. 2006b, JHEP, 06, 053, hep-ph/0605209
 Asaka, T., & Shaposhnikov, M. 2005, Phys. Lett., B620, 17, hep-ph/0505013
 Bahcall, J. N., & Sarazin, C. L. 1977, ApJ, 213, L99, ADS
 Barger, V. D., Phillips, R. J. N., & Sarkar, S. 1995, Phys. Lett., B352, 365, hep-ph/9503295

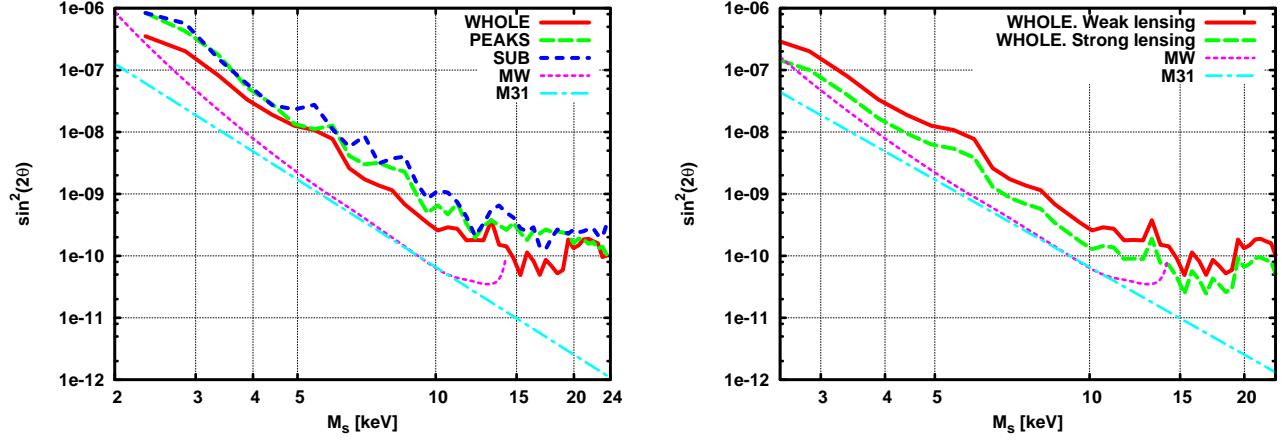


FIG. 7.— (a) Our 3σ limits on sterile neutrino parameters from different spectral regions, using the dark matter masses from weak lensing. The area above the curves is excluded. For comparison, XMM constraints from the Milky Way (Boyarisky et al. 2006d) and M31 (Watson et al. 2006) are shown. (b) Our constraints for region WHOLE using masses determined from weak lensing (same as in panel a) and strong lensing.

Bartelmann, M., & Schneider, P. 2001, Phys. Rep., 340, 291, ADS, astro-ph/9912508
 Biermann, P. L., & Kusenko, A. 2006, Phys. Rev. Lett., 96, 091301, astro-ph/0601004
 Bode, P., Ostriker, J. P., & Turok, N. 2001, Astrophys. J., 556, 93, astro-ph/0010389
 Boyarsky, A., Neronov, A., Ruchayskiy, O., & Shaposhnikov, M. 2006a, MNRAS, 370, 213, ADS, astro-ph/0512509
 —. 2006b, JETP Letters, 133, hep-ph/0601098
 —. 2006c, Phys. Rev. D, 74, 103506, astro-ph/0603368
 Boyarsky, A., Neronov, A., Ruchayskiy, O., Shaposhnikov, M., & Tkachev, I. 2006d, astro-ph/0603660
 Boyarsky, A., Nevalainen, J., & Ruchayskiy, O. 2006e, astro-ph/0610961
 Bradač, M., et al. 2006, astro-ph/0608408
 Cavaliere, A., & Fusco-Femiano, R. 1976, A&A, 49, 137, ADS
 Clowe, D., Bradač, M., Gonzalez, A. H., Markevitch, M., Randall, S. W., Jones, C., & Zaritsky, D. 2006, ApJ, 648, L109, ADS
 Dodelson, S., & Widrow, L. M. 1994, Phys. Rev. Lett., 72, 17, hep-ph/9303287
 Dolgov, A. D., & Hansen, S. H. 2002, Astropart. Phys., 16, 339, hep-ph/0009083
 Goerdt, T., Moore, B., Read, J. I., Stadel, J., & Zemp, M. 2006, MNRAS, 368, 1073, ADS, astro-ph/0601404
 Hansen, S. H., Lesgourgues, J., Pastor, S., & Silk, J. 2002, MNRAS, 333, 544, astro-ph/0106108
 Hickox, R. C., & Markevitch, M. 2006, ApJ, 645, 95, ADS, astro-ph/0512542
 Kusenko, A. 2006a, astro-ph/0609375
 —. 2006b, hep-ph/0609081
 Markevitch, M. 2005, astro-ph/0511345

Markevitch, M. et al. 2003, ApJ, 583, 70, ADS, astro-ph/0209441
 Markevitch, M., & et al. 2006, in preparation
 Pal, P. B., & Wolfenstein, L. 1982, Phys. Rev., D25, 766
 Protassov, R., van Dyk, D. A., Connors, A., Kashyap, V. L., & Siemiginowska, A. 2002, ApJ, 571, 545, ADS, astro-ph/0201547
 Riemer-Sørensen, S., Hansen, S. H., & Pedersen, K. 2006, ApJ, 644, L33, ADS, astro-ph/0603661
 Riemer-Sørensen, S., Pedersen, K., Hansen, S. H., & Dahle, H. 2006, astro-ph/0610034
 Seljak, U., Makarov, A., McDonald, P., & Trac, H. 2006, astro-ph/0602430
 Shaposhnikov, M., & Tkachev, I. 2006, Phys. Lett., B639, 414, hep-ph/0604236
 Smith, R. K., Brickhouse, N. S., Liedahl, D. A., & Raymond, J. C. 2001, ApJ, 556, L91, ADS, astro-ph/0106478
 Stasielak, J., Biermann, P. L., & Kusenko, A. 2006, astro-ph/0606435
 Strigari, L. E., et al. 2006, astro-ph/0603775
 Strumia, A., & Vissani, F. 2006, hep-ph/0606054
 Tremaine, S., & Gunn, J. E. 1979, Phys. Rev. Lett., 42, 407
 Viel, M., Lesgourgues, J., Haehnelt, M. G., Matarrese, S., & Riotto, A. 2005, Phys. Rev., D71, 063534, astro-ph/0501562
 —. 2006, Phys. Rev. Lett., 97, 071301, astro-ph/0605706
 Vikhlinin, A., Kravtsov, A., Forman, W., Jones, C., Markevitch, M., Murray, S. S., & Van Speybroeck, L. 2006, Astrophys. J., 640, 691, ADS, astro-ph/0507092
 Watson, C. R., Beacom, J. F., Yuksel, H., & Walker, T. P. 2006, Phys. Rev., D74, 033009, astro-ph/0605424
 Weisskopf, M. C., Brinkman, B., Canizares, C., Garmire, G., Murray, S., & Van Speybroeck, L. P. 2002, PASP, 114, 1, ADS, astro-ph/0110308